Electrically Driven Multiaxis Rotational Dynamics of Colloidal Platelets in Nematic Liquid Crystals

Clayton P. Lapointe,[1,2] Sharla Hopkins,[1] Thomas G. Mason,[2] and Ivan I. Smalyukh[1,3,*]

[1]*Department of Physics and Liquid Crystals Materials Research Center, University of Colorado at Boulder, Boulder, Colorado 30309, USA*

[2]*Department of Chemistry and Biochemistry, Department of Physics and Astronomy, and California Nanosystems Institute, University of California at Los Angeles, Los Angeles, California 90095, USA*

[3]*Renewable and Sustainable Energy Institute, University of Colorado at Boulder, Boulder, Colorado 30309, USA*

(Received 24 April 2010; published 18 October 2010)

We describe field-induced multiaxis rotations of colloids in a nematic liquid crystal. Anchoring of the nematic director to the colloidal platelet's surface and interplay of dielectric and elastic energies enable robust control over colloid orientation that cannot be achieved in isotropic liquids. Because of the anisotropy of the fluid and the platelike shape of particles, the colloids can be forced to rotate about four different rotational axes even for a fixed direction of the applied field. The time scale of these unexpected voltage-dependent dynamics varies over four orders of magnitude (10^{-2}–10^{2} s) and promises a number of novel electro-optic, photonic, and display applications.

DOI: 10.1103/PhysRevLett.105.178301 PACS numbers: 82.70.Dd, 47.57.−s, 61.30.Gd

Colloids suspended in nematic liquid crystals (NLCs) are a fascinating type of soft matter extending the scope of colloidal science to include many intricacies in the physics of liquid crystals, such as elasticity, topological defects, and anisotropic hydrodynamics [1]. The long-range orientational order of nematic hosts generates elasticity-mediated colloidal interactions that cannot occur in isotropic liquids [1]. The NLC's facile response to external fields allows for the control of topological defects and molecular alignment around the colloidal inclusions described by the director field $\mathbf{n}(\mathbf{r})$ [2]. Through surface anchoring and elasticity of the NLC host, the orientations of nonspherical colloids couple strongly to $\mathbf{n}(\mathbf{r})$, allowing for their alignment and shape-dependent self-assembly [3]. The ensuing colloidal systems exhibit long-range orientational order of anisotropic particles and are of interest for the design of new composites such as optical metamaterials [2,3]. Self-assembled tunable metamaterials may potentially be realized through the NLC-mediated realignment and rearrangement of incorporated particles and are of interest for applications ranging from nanoscale optical imaging to invisibility cloaking. Making a metamaterial requires manipulating self-assembly of complex anisotropic colloids, such as toroids, coupled rods, and split rings [3–5], as well as controlling their orientations. However, in both isotropic and nematic hosts, the demonstration of such field-driven control is scarce and limited to colloids with highly symmetric shapes and to rotations around a single axis predetermined by the field direction [4].

In this Letter, we describe electrically driven multiaxis rotations of model platelet colloids in a NLC. Unexpectedly, depending on the applied voltage, the colloids reversibly rotate around four different axes, even though the direction of the applied external field is constant. Using a simple model that considers the interplay of elastic, dielectric, and viscous torques, we show that the particle shape and NLC anisotropy are the salient features of this unexpectedly rich landscape of mechanical response.

We use photolithography to fabricate custom-designed square platelet colloids out of SU-8 photoresist having an edge length $L = 4.5$ μm, thickness $h = 1$ μm, and a centered square hole with 2 μm sides [Fig. 1] [3]. This particular shape was chosen to enhance the particle's mechanical coupling to the NLC by increasing the surface-to-volume ratio at a given lateral size. The colloids are added at low concentration to two NLCs with positive dielectric anisotropy $\Delta\varepsilon = \varepsilon_{\parallel} - \varepsilon_{\perp}$: ZLI-3412 (EM Industries) with $\Delta\varepsilon = 3.9$, $\varepsilon_{\parallel} = 7.3$ and pentylcyanobiphenyl (5CB) with $\Delta\varepsilon = 11$, $\varepsilon_{\parallel} = 18.1$. Sample cells consist of glass plates coated with transparent indium tin oxide and rubbed polyimide alignment layers (PI-2555) spaced by 10 μm glass beads. Polyimide induces strong planar anchoring of $\mathbf{n}(\mathbf{r})$ along the rubbing direction with a small pretilt angle $\approx$ 1–2°. Rubbing directions at the top and bottom plates are set antiparallel so that initially, the director is everywhere uniform [$\mathbf{n}(\mathbf{r}) \parallel \hat{\mathbf{x}}$] and coherently rotates counterclockwise about $\hat{\mathbf{y}}$ in response to applied voltages [Fig. 1(e)]. Sinusoidal voltages at 1 kHz are applied across the indium tin oxide electrodes of the cell using a function generator (DS340, Stanford Research Systems). We use an inverted microscope (IX-81, Olympus) equipped with a laser scanning confocal unit (FV300, Olympus), allowing for 3D imaging of $\mathbf{n}(\mathbf{r})$ using fluorescence confocal polarization microscopy (FCPM) [3]. The rotational dynamics of isolated platelets are probed using high-speed video microscopy (HotShot 512sc, Photosonics) and image analysis is extended to extract the orientation data and is cross-correlated with

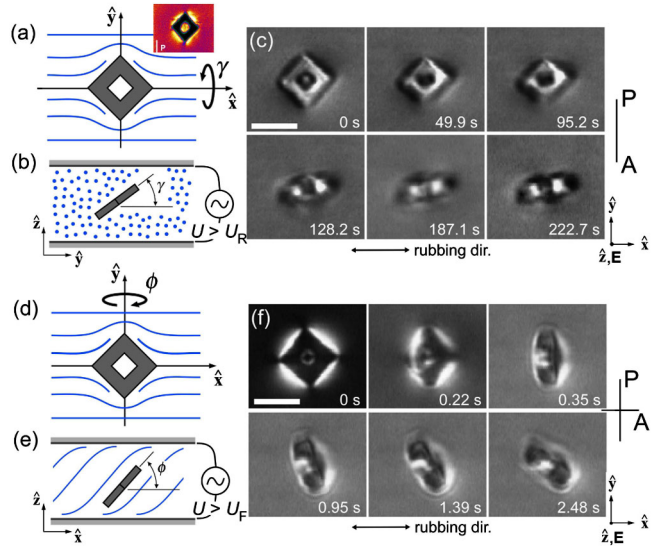

FIG. 1 (color online). Voltage-dependent multiaxis rotation of a colloidal platelet at (a)–(c) $U < U_F$ and (d)–(f) $U > U_F$. (a) A square platelet with quadrupolar $\mathbf{n}(\mathbf{r})$ at $U = 0$ and definition of the angle γ; the inset shows a FCPM image (obtained for the polarization of probing light perpendicular to the far-field director) of the $\mathbf{n}(\mathbf{r})$ "corona" around the platelet. (b) Schematic side view of the cell in the $\hat{\mathbf{y}}$-$\hat{\mathbf{z}}$ plane and (c) video frames showing a rotation about $\hat{\mathbf{x}}$ (increasing γ) from lying in-plane $\gamma = 0$ to upright orientation ($\gamma = \pi/2$) at $U \approx U_R = 1.2$ V. (d) At $U > U_F$, rotations are about the y axis (increasing ϕ). (e) Schematic in the $\hat{\mathbf{x}}$-$\hat{\mathbf{z}}$ plane showing the tilt angle ϕ and deformations of $\mathbf{n}(\mathbf{r})$. (f) Video frames showing the platelet's initial fast rotation about $\hat{\mathbf{y}}$ followed by a slower rotation about $\hat{\mathbf{z}}$ while upright ($U = 6$ V). Background intensity changes under crossed polarizers as the NLC is switched.

the FCPM studies. Because of the advantages of using a low-birefringence NLC for FCPM imaging, the results in this Letter are reported for colloids in a nematic ZLI-3412 with $\Delta n \approx 0.08$, although we observe qualitatively similar behavior for colloids in 5CB.

In a planar NLC cell, square platelets align with one diagonal axis parallel to the rubbing direction ($\parallel \hat{\mathbf{x}}$), inducing quadrupolar $\mathbf{n}(\mathbf{r})$ deformations [3], as shown in Fig. 1(a). This alignment is robust; thermally driven angular fluctuations of the square's diagonal axis relative to $\hat{\mathbf{x}}$ have a narrow Gaussian distribution having width $<1°$. Although continuous rotations of the platelet-$\mathbf{n}(\mathbf{r})$ quadrupolar structure about $\hat{\mathbf{x}}$ are energetically invariant in an infinite NLC, the proximity of the bounding surfaces lifts this degeneracy, and platelets align with their large-area faces parallel to the glass plates. While observing an isolated colloid using video microscopy, the amplitude of the driving voltage U is gradually increased from zero. Below a threshold $U < U_R \approx 1.2$ V, no response of the colloid to the applied field is observed. For $U_R < U < U_F$, where $U_F = 2.4$ V is the Fréedericksz threshold voltage for the bulk realignment of $\mathbf{n}(\mathbf{r})$, the applied field induces a slow rotation of the platelet about $\hat{\mathbf{x}}$ [increasing γ, Figs. 1(a) and 1(b)] to an upright orientation ($\gamma \approx \pi/2$). As shown in Fig. 1(c), during this rotation, NLC elasticity constrains one of the colloid's diagonal axes to lie parallel to $\hat{\mathbf{x}}$, and upon reaching $\gamma \approx \pi/2$, the other diagonal aligns parallel to the field direction ($\parallel$ to $\hat{\mathbf{z}}$). This rotation takes place at a voltage well below U_F, so that $\mathbf{n}(\mathbf{r})$ away from the colloid remains intact.

Even when suspended in isotropic fluids, nonspherical colloids experience electric field-induced torques due to shape anisotropy if the dielectric constant ε of the particle and fluid differ [4]. Since SU-8 has a lower ε at 1 kHz ($\varepsilon_{\text{SU-8}} \approx 3.0$) [5] than ZLI-3412 in the planar cell ($\varepsilon_\perp \approx 3.4$), a torque due to shape anisotropy tends to align the platelet perpendicular to the field, and therefore, the observed rotation is unexpected. However, surface anchoring pins $\mathbf{n}(\mathbf{r})$ tangential to the SU-8–NLC interface, forming a dielectrically anisotropic "corona" around the colloid that extends away from the colloid to distances comparable to the particle size. The corona's dielectric anisotropy energetically favors aligning the platelet's diagonal axis (the one originally parallel to $\hat{\mathbf{y}}$) parallel to the electric field $\mathbf{E}$. In particular, when the platelet is lying in-plane ($\gamma = 0$), $\mathbf{n}(\mathbf{r})$ within the corona is everywhere orthogonal to $\mathbf{E}$ and the effective dielectric constant is $\varepsilon_\perp$, but after the platelet rotates to $\gamma = \pi/2$, $\mathbf{n}(\mathbf{r})$ at the platelet's edges are at $\pi/4$ relative to $\mathbf{E}$. The latter orientation reduces the dielectric term of the NLC free energy, $F_E = -(\varepsilon_0 \Delta\varepsilon/2) \int d^3\mathbf{r}[\mathbf{E} \cdot \mathbf{n}(\mathbf{r})]^2$ [8], where ε_0 is the dielectric permittivity of free space. A competition between elastic and dielectric energies defines the observed threshold voltage U_R, since rotations from $\gamma = 0$ to $\gamma = \pi/2$ are resisted by the elastic interaction responsible for the platelet to align with its larger-area faces parallel to the cell substrates at $U = 0$ [6]. Furthermore, the torque on the corona competes with an opposing torque due to the dielectric contrast between lower-ε SU-8 platelet and higher-ε NLC resulting in a slow response above U_R.

Significantly faster and more complex rotations are possible if U is increased above the Fréedericksz threshold $U > U_F = 2.4$ V [Fig. 1(f)]. The director rotates in response to the field while mechanical coupling via surface anchoring torques the platelet upright to a certain tilt angle ϕ. The counterclockwise sense of the colloid's rotation about $\hat{\mathbf{y}}$ always matches that of $\mathbf{n}(\mathbf{r})$, which is determined by director pretilt at substrates [Fig. 1(e)]. An additional slower in-plane rotation about $\hat{\mathbf{z}}$ accompanies the out-of-plane rotation about $\hat{\mathbf{y}}$ over the range $2.4 \text{ V} \leq U \leq 4.5$ V [Fig. 2(a)], but they decouple in time for $U > 5$ V [Fig. 2(b)]. Switching the field off results in $\mathbf{n}(\mathbf{r})$ relaxing to the uniform planar state, and the platelet, consequently, rotates back to its equilibrium alignment at $\phi = \gamma = 0$ [9]. Using high-speed video microscopy and image analysis, we have measured the platelet's tilt angle ϕ as a function of time at various U, as shown for $U = 6$ V and 10 V in Fig. 2(c). These trajectories can be fit reliably over the whole range with a sigmoid function, $\phi(t) = \phi_0/\{1 + \exp[-(t - t_0)/\tau_\phi]\}$ where ϕ_0 is the total

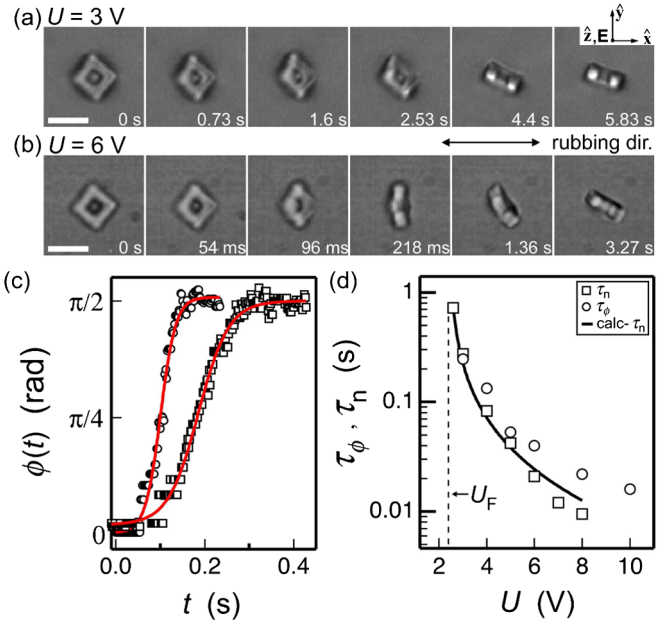

FIG. 2 (color online). Fast out-of-plane rotations at $U > U_F$. (a) In response to an applied voltage just above U_F ($U = 3$ V), the platelet rotates simultaneously about $\hat{\mathbf{y}}$ and $\hat{\mathbf{z}}$. (b) At $U \geq 6$ V, these rotations decouple in time. (c) Platelet tilt angle $\phi(t)$ for $U = 6$ V (squares) and $U = 10$ V (circles). Solid (red) curves show fits to the data with sigmoid trajectories. (d) Relaxation time τ_ϕ as a function of U extracted from the $\phi(t)$ data. Corresponding switching times τ_n of the same cell are shown for comparison. Vertical dashed line indicates $U_F = 2.4$ V. The solid curve shows expected U dependence of τ_n.

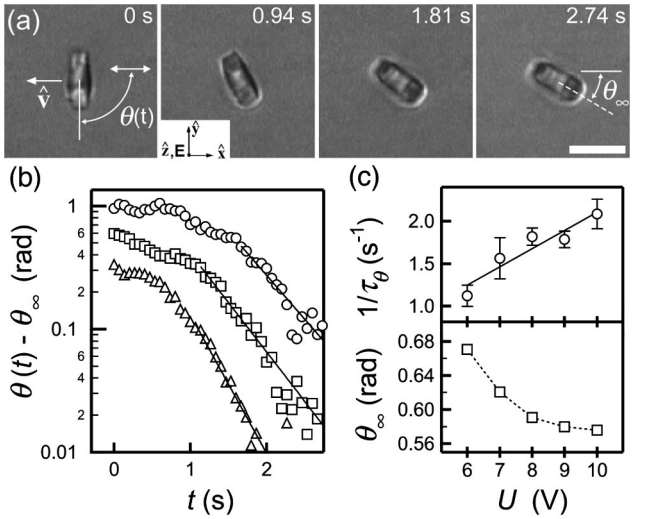

FIG. 3. In-plane rotations due to interactions with the near-surface deformations of $\mathbf{n}(\mathbf{r})$. (a) After flipping upright, a rotation about $\hat{\mathbf{z}}$ (decreasing θ) orients the platelet's projected long axis to an equilibrium angle θ_∞ relative to the rubbing direction (white arrow). (b) Trajectories $\theta(t) - \theta_\infty$ for $U = 6$ (circles), 8 (squares), and 10 V (triangles); late-time exponential fits (solid lines) yield the decay times τ_θ. (c) $1/\tau_\theta$ (top) and θ_∞ (bottom) as a function of U.

change of $\phi(t)$, t_0 is the time at which $\phi(t_0) = \phi_0/2$, and τ_ϕ is a relaxation time. For each U, we extract τ_ϕ from five trajectories and average them to obtain τ_ϕ as a function of U [Fig. 2(d)]. The statistical uncertainty of τ_ϕ is less than 10% at all voltages. For comparison, we measured the respective switching times of the NLC, τ_n, optically within the same cell. As shown by the solid line in Fig. 2(d), data for τ_n agree with the expected voltage dependence: $\tau_n = (\eta_R d^2/\pi^2 K)[(U/U_F)^2 - 1]^{-1}$, where $\eta_R = 0.146$ Pa · s is the rotational viscosity, $K = 12.1$ pN is the average Frank elastic constant of ZLI-3412, and $d = 11$ μm is the cell gap. At low U, τ_ϕ closely follows the voltage dependence of τ_n, indicating that the mechanical coupling of the platelet's orientation to the local $\mathbf{n}(\mathbf{r})$ is strong. Above $U = 5$ V, the difference between τ_ϕ and τ_n increases with increasing U due to growing viscous dissipation associated with shear flow and backflow (arising from director reorientation), which are both expected to systematically increase τ_ϕ relative to τ_n. Since $\tau_n \propto d^2$, cell thickness allows one to control τ_ϕ and also the time scale of rotations around the other axes.

At high voltages above $U = 5$ V, rotational motion about $\hat{\mathbf{y}}$ ceases after reaching $\phi = \pi/2$, and is followed by a rotation about $\hat{\mathbf{z}}$ [decreasing θ, Fig. 3(a)] as well as a $\pi/4$ rotation about a body frame vector $\hat{\mathbf{v}}$ orthogonal to the platelet's larger-area faces. The latter rotation can be seen in Fig. 3(a), wherein the projected image of the upright platelet decreases from the length of a diagonal (6.4 μm) to that of a side (4.5 μm). At $U > U_F$, the colloid also translates vertically from the middle of the cell to the near-substrate region with splay-bend deformations occurring over a height $\zeta \sim (d/U)[K/(\varepsilon_0 \Delta\varepsilon)]^{1/2} \sim d(U_F/U)$ [8]. The rotational and translational motion is seen in vertical confocal sections through the upright platelet [left side, Fig. 4] obtained with FCPM polarization $\mathbf{P}_{\mathrm{FCPM}} \perp \hat{\mathbf{x}}$, for which the background NLC is dark and the square's position and orientation is imaged using fluorescence arising from the $\mathbf{n}(\mathbf{r})$ deformations near its edges. For comparison, the right-side FCPM sections in Figs. 4(b)–4(d) are taken away from the particle and with $\mathbf{P}_{\mathrm{FCPM}} \parallel \hat{\mathbf{x}}$, so that the fluorescence texture indicates spatial changes of the tilt angle $\alpha(\mathbf{r})$ and $\mathbf{n}(\mathbf{r}) = \cos\alpha(\mathbf{r})\hat{\mathbf{x}} + \sin\alpha(\mathbf{r})\hat{\mathbf{z}}$. The splay-bend deformations are visible as bright bands of width ζ at the top and bottom of the cell.

The platelet's translation and rotation can be understood using simple considerations. Initially, due to strong elastic $\mathbf{n}(\mathbf{r})$ gradients and $\mathbf{n}(\mathbf{r})$ being not parallel to $\mathbf{E}$, the regions near the cell substrates and next to the upright square's edges in the cell midplane are costly in both elastic and dielectric energies. The field-induced translation toward the substrate and the $\pi/4$ rotation about $\hat{\mathbf{v}}$ [Fig. 4] decreases the distortions between the cell substrate and the platelet's edge, lowering the overall free energy. While becoming partially immersed into the ζ-thick layer, which contains a significant $\hat{\mathbf{x}}$ component of $\mathbf{n}(\mathbf{r})$, the platelet's rotation about $\hat{\mathbf{z}}$ from $\theta = \pi/2$ to the equilibration angle $\theta = \theta_\infty$

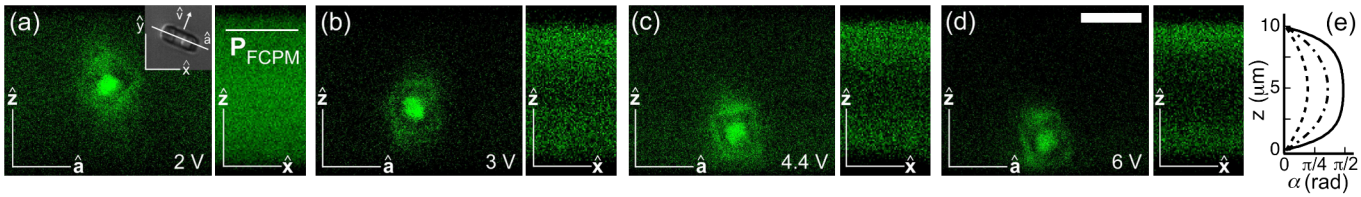

FIG. 4 (color online). FCPM cross sections in the $\hat{\mathbf{a}}$-$\hat{\mathbf{z}}$ plane (left, see inset) and $\hat{\mathbf{x}}$-$\hat{\mathbf{z}}$ plane (right) at various U. For the $\hat{\mathbf{a}}$-$\hat{\mathbf{z}}$ scans, FCPM polarization is $\mathbf{P}_{\mathrm{FCPM}} \parallel \hat{\mathbf{y}}$ and $\mathbf{P}_{\mathrm{FCPM}} \parallel \hat{\mathbf{x}}$ in the $\hat{\mathbf{x}}$-$\hat{\mathbf{z}}$ scans. (a) At $U = 2$ V, after rotating by $\pi/2$ about $\hat{\mathbf{x}}$, the square remains in the bulk of the cell with a diagonal axis along $\hat{\mathbf{z}}$. Inset: Definition of the $\hat{\mathbf{a}}$-$\hat{\mathbf{z}}$ cross sections (white line). (b) At $U = 3$ V just above U_F, the platelet translates downward and rotates by $\pi/4$ about $\hat{\mathbf{v}}$. (c) At $U = 4.4$ V and (d) $U = 6$ V, the square is pulled to the substrate and the size of the near-surface layer (bright regions on right) becomes comparable to the size of the colloid. (e) Calculated $\alpha(z)$ for $U = 3$ (dashed), 4.4 (dotted-dashed), and 6 V (solid).

[Fig. 3(a)] further decreases the elastic energy while accommodating the tangential boundary conditions at the platelet's four vertical faces (two larger-area faces and two edge faces). We have observed similar rotations using 5CB that can result in much smaller $\theta_\infty \approx 0$. This likely arises from 5CB's lower average elastic constant ($K \approx 7$ pN) and significantly larger dielectric anisotropy ($\Delta\varepsilon \approx 11$).

Using image analysis, we probe the dynamics of rotations about $\hat{\mathbf{z}}$ by tracking the rotation of platelet's projected long axis in the $\hat{\mathbf{x}}$-$\hat{\mathbf{y}}$ plane as it decreases from $\theta = \pi/2$ to the equilibrium $\theta_\infty \geq 0$ [Fig. 3(a)]. Angular trajectories for $U = 6$, 8, and 10 V are shown in Fig. 3(b). At late times, the relaxation is exponential and we characterize the dynamics by fitting with $\theta(t) - \theta_\infty = \theta_0 \exp(-t/\tau_\theta)$ over the range $0 \leq \theta(t) - \theta_\infty \leq 0.2$ rad. The decay time τ_θ and the equilibrium angle θ_∞ decrease monotonically with increasing U [Fig. 3(c)]. Although we do not expect a dielectric torque on the particle when it is already aligned parallel to the field direction, this in-plane rotation arises from the elastic interaction of the particle-induced distortions of $\mathbf{n}(\mathbf{r})$ and field-dependent director deformations near the surface. Thus, θ_∞ is dependent on the characteristic thickness of the near-surface region ζ which, in turn, depends on U. The excess elastic energy $\sim KLh/\zeta$ that drives rotations from $\theta = \pi/2$ to $\theta = \theta_\infty$ arises from the $\mathbf{n}(\mathbf{r})$ deformations concentrated between the upright square platelet and the substrate. To understand the time scales and voltage dependence of this rotation, we Taylor expand the elastic free energy $F_{\mathrm{el}}(\theta)$ around the minimum at $\theta = \theta_\infty$ and obtain $F_{\mathrm{el}}(\theta) \approx K(Lh/\zeta)(\theta - \theta_\infty)^2/2$. Since the Reynolds number is small ($\mathrm{Re} \sim 10^{-7}$), inertia is negligible. In addition, the Erickson number is small so that perturbations to $\mathbf{n}(\mathbf{r})$ from fluid flow can be ignored and the elastic torque $\Gamma_{\mathrm{el}} = -\partial F_{\mathrm{el}}/\partial\theta \approx -K(\theta - \theta_\infty)Lh/\zeta$ is balanced by a viscous drag torque $\Gamma_v = \sigma\eta\dot{\theta}$, where σ is a rotational drag coefficient and η is an effective shear viscosity coefficient. Solutions of the equation of motion are exponential: $\theta(t) = \theta_0 \exp(-t/\tau_\theta) + \theta_\infty$, where the decay time is $\tau_\theta = \sigma\eta\zeta/(KLh)$, the drag coefficient is approximated as $\sigma \sim D^3$ (although this is a crude approximation as the rotational drag coefficient for a platelet in the NLC is anisotropic) with $D = 6.4$ μm being the diagonal length of the square, and values of ζ range from hundreds of nanometers to several micrometers (depending on U). Thus, one obtains a linear dependence of $1/\tau_\theta$ on U with a slope $KLh\sqrt{\varepsilon_0\Delta\varepsilon/K}/(\eta dD^3) \approx 0.52$ s^{-1} V^{-1}, where we have used experimental values of $K = 12.1$ pN, $d = 11$ μm, and $\eta = 0.04$ Pa $\cdot$ s. Despite of a number of approximations, this value is close to the slope of 0.22 ± 0.04 s^{-1} V^{-1} determined from a fit shown in Fig. 3(c).

In conclusion, we have demonstrated that a platelike colloidal particle immersed in a nematic liquid crystal can be driven about multiple rotational axes by applying a unidirectional electric field. Similar field-controlled rotations could be achieved for so-called Janus particles and colloids with patchy surface anchoring, as well as using different NLC host media. Controlling these rotations and their time scales via tuning the voltage amplitude may provide a key step in the creation of reconfigurable composites for metamaterial applications [3–5]. Furthermore, since the switchable NLC-colloidal dispersions can be made of particles of different material composition and with various surface coatings, they may find applications in the reflective displays, spatial light modulators, shutters, and beam steering devices [8].

We acknowledge funding from the Institute for Complex Adaptive Matter and NSF (Grants No. DMR-0645461, No. DMR-0847782, and No. CHE-0450022).

*ivan.smalyukh@colorado.edu

[1] P. Poulin, H. Stark, T. C. Lubensky, and D. A. Weitz, Science **275**, 1770 (1997).
[2] J.-I. Fukuda and H. Yokoyama, Mol. Cryst. Liq. Cryst. **475**, 165 (2007).
[3] C. P. Lapointe, T. G. Mason, and I. I. Smalyukh, Science **326**, 1083 (2009).
[4] V. G. Veselago, Sov. Phys. Usp. **10**, 509 (1968).
[5] J. B. Pendry, Phys. Rev. Lett. **85**, 3966 (2000).
[6] T. B. Jones, *Electromechanics of Particles* (Cambridge University Press, New York, 1995).
[7] S. Arscott *et al.*, Electron. Lett. **35**, 243 (1999).
[8] C. Yeh and C. Gu, *Optics of Liquid Crystal Displays* (Wiley & Sons, New York, 1999).
[9] See supplementary material at http://link.aps.org/supplemental/10.1103/PhysRevLett.105.178301 to view a video that shows the rotation of the platelet at various U.